

## Collisions of electrons with trimethylamine $\text{N}(\text{CH}_3)_3$ molecules

Czesław Szmytkowski,\* Alicja Domaracka, Paweł Możejko, and Elżbieta Ptasńska-Denga  
*Atomic Physics Group, Faculty of Applied Physics and Mathematics, Gdańsk University of Technology,  
 ul. G. Narutowicza 11/12, 80-952 Gdańsk, Poland*  
 (Received 1 March 2007; published 31 May 2007)

Absolute total electron-trimethylamine scattering cross section (TCS) has been measured from 0.8 to 370 eV with a linear electron-transmission method. The experimental TCS energy function is dominated by very pronounced enhancement peaked near 9 eV. The present TCS agrees qualitatively with low-energy results of Schmieder [Z. Elektrochem. **36**, 700 (1930)] but there are substantial differences in the position and peak values. Calculations were also carried out to obtain the integral elastic and ionization cross sections at intermediate and high energies using the independent atom (IAM) and the binary-encounter-Bethe (BEB) approximations, respectively. Their sum, the estimated total cross section, is for intermediate energies in a reasonable agreement with the present experimental TCS data. Furthermore, the measured TCS for  $\text{N}(\text{CH}_3)_3$  is compared with the TCSs for other nitrous compounds:  $\text{NH}_3$  and  $\text{NH}_2\text{CH}_3$ . The variation of the TCS magnitude across the series of nitrogen-containing molecules [ $\text{NH}_3$ ,  $\text{NH}_2\text{CH}_3$ , and  $\text{N}(\text{CH}_3)_3$ ] is explained in terms of their molecular size.

DOI: [10.1103/PhysRevA.75.052721](https://doi.org/10.1103/PhysRevA.75.052721)

PACS number(s): 34.80.Bm, 34.80.Gs

### I. INTRODUCTION

Trimethylamine [TMA,  $\text{N}(\text{CH}_3)_3$ ] is a volatile organic compound which is released into the environment from the chemical plant industry, marine meal manufacturers [1], or emitted during cremation [2]. Beside the specific malodorous property, TMA is dangerous for animals and human beings because of its tissue corrosive and penetrative properties. TMA has been shown to be an inhibitor of DNA, RNA, and proteins synthesis, and it has teratogenic effect on animal embryos [3]. Due to its odor and high toxicity, the removal of TMA from exhaust becomes a top priority. A promising method of gas mixture purification is based on removal of toxic compounds by electron-driven techniques. Designing and construction of efficient separation reactors employing electron sources needs, however, comprehensive electron-scattering data.

There are, to date, few experimental studies of electron interactions with trimethylamine. The only previous total cross section measurement was recorded in the early 1930s [4]. Later works were concerned with the high-energy electron diffraction [5], the electron swarm transport [6], the dissociative ionization [7,8], and the low-energy electron transmission spectroscopy [9,10]. More recent studies of TMA involving electrons as projectile focused mainly on processes with molecules adsorbed on solid substrates: as electron-induced vibrational excitation of TMA molecules chemisorbed on GaAs(100) [11], or decomposition of TMA adsorbed on Si(100) [12,13]. Only experiments of Schmieder [4] and Christophorou and Christodoulides [6] provided absolute values of the scattering intensities. Theoretical results concerning the electron-assisted processes with TMA have not been reported in the literature as yet.

In this paper, we report the absolute electron-scattering total cross section measured from 0.8 to 370 eV, and the

integrated elastic and ionization cross sections calculated at intermediate and high energies. As the electron-trimethylamine scattering total cross section (TCS) is obtained without any normalization procedure, it is one of the most reliable quantity describing the scattering. Therefore, the absolute TCS can be a valuable, quantitative test of theoretical models and computational procedures. On the other hand, the regularities and features discerned in the TCS energy function may be a stimulus for further, more refined experimental and theoretical studies on  $e\text{-N}(\text{CH}_3)_3$  scattering.

### II. EXPERIMENTAL PROCEDURE AND SETUP

The present absolute total  $e\text{-N}(\text{CH}_3)_3$  scattering cross section (TCS) has been measured using the electron-transmission method in a linear configuration, under single scattering conditions. This method relates the TCS to the attenuation of an electron current by the target molecules filling the reaction volume. The apparatus and measuring procedure used in the present experiment has been discussed in detail before [14,15], so only a brief summary will be given here. The electron beam was filtered by a  $127^\circ$ -cylindrical electrostatic monochromator and focused into the interaction region at the required energy  $E$  with a resolution of about 100 meV. The electrons emerging from the cell exit aperture are energy discriminated by a retarding-field lens unit and eventually collected with a Faraday cup. A magnetic field along the pathway of electrons has been reduced below  $0.1 \mu\text{T}$ , and ensured the trajectory of unscattered electrons to be a straight line within the scattering region.

The parameters directly recorded in the experiment are the following:  $I(p, E)$  and  $I(p=0, E)$ —the intensities of the transmitted electron currents in the presence and absence of the target gas in the scattering cell, respectively;  $p$ —the pressure of the investigated target gas in the cell of the length  $L$  ( $=30.5 \text{ mm}$ ); and  $T_c$ —the temperature of the scattering cell ( $305\text{--}320 \text{ K}$ ). The electron energy scale is calibrated with an

\*Electronic address: [czsz@mif.pg.gda.pl](mailto:czsz@mif.pg.gda.pl)

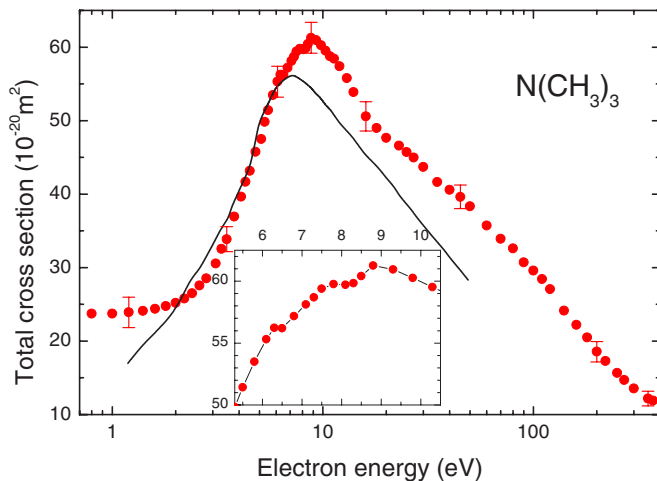


FIG. 1. (Color online) Experimental total cross sections for  $e$ - $N(\text{CH}_3)_3$  scattering. Full circles are the present measurements (error bars represent overall experimental uncertainties), while the full line shows pioneering data of Schmieder [4]. The inset highlights the present TCS features (note the linear energy scale); the line is added to guide the eye.

accuracy of about 0.1 eV against the oscillatory structure visible around 2.3 eV in the transmitted current when molecular nitrogen is admixed to the compound under study. The total cross section  $Q(E)$  at each energy  $E$  is then derived using the Bouguer-de Beer-Lambert (BBL) attenuation relationship

$$I(p, E) = I(p = 0, E) \exp\left(-\frac{pL}{k\sqrt{T_m T_c}} Q(E)\right),$$

in which the thermal transpiration effect [16] is accounted for;  $T_m$  (=322 K) is the temperature of the mks capacitance manometer head and  $k$  is the Boltzmann constant.

The final value of the experimental TCS at each particular energy (as presented in Table II and Fig. 1) is an average of a large number of data obtained in series (3–8) of individual runs (8–10 in a series). The statistical uncertainty of TCS results (one standard deviation of the weighted mean value) is usually well below 1%, excluding the lowest and highest energies employed, i.e., below 1 eV and above 200 eV, where the uncertainty increases to almost 2%.

The systematic uncertainty in the present experiment is of great importance for accurate TCS determination. Among the effects which may distort the measured TCS systematically, two are inherently associated with the electron-transmission technique applied, and are due to difficulties to meet exactly the conditions at which the BBL formula is valid. The first one relates to the imperfect discrimination, by the detector system, of electrons scattered into small forward angles that systematically lowers the obtained TCS values. Generally, the forward scattering of electrons increases at higher impact energies although, for polar molecules (see Table IV), it is also important at low collision energies. The extent to which such scattering effects may reduce the measured cross section may be estimated if the elastic differential scattering cross section is known. We used our calculations (described

below) to estimate the effect at intermediate energies. At low energies, due to lack of pertinent data, the estimation is based only on comparison with other molecules of similar size and the electric dipole moment value. For the present geometry of the electron collector system, the lessening of the measured TCS should not exceed 2–3% at the lowest and highest applied energies. The second factor affecting the measured TCS is connected with the effusion of target molecules throughout the entrance and exit apertures of the scattering cell. This unavoidable end effect does not allow an accurate determination of the numerator  $pL$  in the BBL formula. The uncertainty related to that factor was estimated to be lower than 2.5% (cf. Ref. [17]), while an accuracy of the pressure  $p$ , measured with the mks capacitance manometer, amounts of about 1%. To reduce the influence of the target molecules (effusing from the reaction cell) on the electron optics and, in consequence, on the intensity of the primary electron beam, the target was allowed alternately into the scattering cell and the electron optics volume in such a way that the partial target pressure in the electron optics region was constant, irrespective of whether the target was present or not in the scattering cell. The overall systematic uncertainty in the measured TCS is about 5–7% below 2 eV, decreasing gradually to 3% between 5–150 eV, and increasing again up to 6% at the highest energies applied.

The sample of  $N(\text{CH}_3)_3$  supplied from Aldrich (99% stated purity) was used without further purification other than vacuum distillation.

### III. THEORETICAL METHODS

To obtain the total cross section for the  $e$ - $N(\text{CH}_3)_3$  scattering beyond the energy range of the existing experiments, computations of the elastic and ionization cross sections have been carried out. The elastic cross section (ECS) for electron collision with molecule studied has been calculated with the independent atom method (IAM) [18], while the electron-impact ionization cross section (ICS) has been obtained within the binary-encounter-Bethe (BEB) formalism [19,20]. The sum of both calculated partial cross sections will represent the computational total cross section. The approximation of the total cross section with the sum of only elastic and ionization components is validated because ionization typically predominates over other inelastic contributions at intermediate and high collision energies. Since the employed theoretical as well as computational methods have been presented in our earlier studies [21,22], only a short description will be provided here.

In the IAM approximation, the electron-molecule collision is reduced to more simple problem of the scattering from individual atomic constituents of target molecule, and the integral elastic cross section for the electron scattering from a molecule is given by

$$\sigma(E) = \frac{4\pi}{k} \sum_{i=1}^N \text{Im} f_i(\theta=0, k) = \sum_{i=1}^N \sigma_i^A(E), \quad (1)$$

where  $E$  is an energy of the incident electron,  $f_i(\theta, k)$  is the scattering amplitude due to the  $i$ th atom of the molecule,  $\theta$  is

TABLE I. Electron binding energies  $B$ , kinetic energies of the orbitals  $U$ , and orbital occupation number  $N$  for a given molecular orbital of  $\text{N}(\text{CH}_3)_3$  molecule.

Molecular orbital	Calc. present	$B$ (eV)		Expt.		$U$ (eV) Calc. present	$N$ Calc. present
		[32]	[33]	[34,35]	[36]		
$1a_1$	305.8					436.0	2
$1e$	305.8					436.0	4
$2a_1$	422.9					602.0	2
$3a_1$	33.43	25.56	30.66	28.3		46.53	2
$2e$	25.94	20.66	23.98	22.5		36.91	4
$4a_1$	21.97	18.18	20.34	19.46		38.11	2
$5a_1$	16.19	14.50	16.08	16.0		26.50	2
$3e$	16.09	14.68	15.84	15.68		30.70	4
$4e$	14.03	13.03	13.75	13.67	14.0	27.99	4
$1a_2$	13.32	12.69	13.11	13.1	12.9	29.58	2
$5e$	12.86	12.17	12.56	12.3, 12.74	12.4	35.99	4
$6a_1$	8.397	9.11	8.56	8.44	8.5	43.40	2

the scattering angle, and  $k = \sqrt{2E}$  is the wave number of the incident electron.

The elastic cross section,  $\sigma_i^A(E)$ , for the  $i$ th atom in the target molecule has been derived according to

$$\sigma^A = \frac{4\pi}{k^2} \left( \sum_{l=0}^{l_{\max}} (2l+1) \sin^2 \delta_l + \sum_{l=l_{\max}}^{\infty} (2l+1) \sin^2 \delta_l^{(B)} \right). \quad (2)$$

To obtain phase shifts,  $\delta_l$ , partial wave analysis has been employed and the radial Schrödinger equation

$$\left\{ \frac{d^2}{dr^2} - \frac{l(l+1)}{r^2} - 2[V_{\text{stat}}(r) + V_{\text{polar}}(r)] + k^2 \right\} u_l(r) = 0 \quad (3)$$

has been solved numerically under the boundary conditions

$$u_l(0) = 0, \quad u_l(r) \xrightarrow{r \rightarrow \infty} A_l \hat{j}_l(kr) - B_l \hat{n}_l(kr), \quad (4)$$

where  $\hat{j}_l(kr)$  and  $\hat{n}_l(kr)$  are the Riccati-Bessel and Riccati-Neumann functions, respectively. Our previous studies [21] have shown that the IAM approach with electron-atom interaction potential composed by static and polarization components can reproduce experimental elastic differential and integral cross sections satisfactorily, at intermediate as well as at high impact energies. Therefore, in the present computations the electron-atom interaction has been also represented by a sum (SP) of static  $V_{\text{stat}}(r)$  [23] and polarization  $V_{\text{polar}}(r)$  [24] potentials only, which are given by following expressions:

$$V_{\text{stat}}(r) = -\frac{Z}{r} \sum_{m=1}^3 \gamma_m \exp(-\beta_m r), \quad (5)$$

where  $Z$  is the nuclear charge of the atom and  $\gamma_m$  and  $\beta_m$  are parameters obtained by the numerical fitting to the Dirac-Hartree-Fock-Slater screening function [23], and

$$V_{\text{polar}}(r) = \begin{cases} \nu(r) & r \leq r_c, \\ -\alpha/2r^4 & r > r_c, \end{cases}$$

where  $\nu(r)$  is the free-electron-gas correlation energy [25],  $\alpha$  is the static electric dipole polarizability of atom, and  $r_c$  is the first crossing point of the curves of  $\nu(r)$  and  $-\alpha/2r^4$  [26].

The phase shifts  $\delta_l$  are connected with an asymptotic form [Eq. (4)] of the wave function  $u_l(r)$  by

$$\tan \delta_l = \frac{B_l}{A_l}. \quad (6)$$

The exact phase shifts have been calculated for  $l$  up to  $l_{\max} = 50$ , while those remaining,  $\delta_l^{(B)}$ , have been included through the Born approximation.

According to the BEB model [19,20] the electron-impact ionization cross section per molecular orbital  $\sigma^{\text{BEB}}$  is given by

$$\sigma^{\text{BEB}} = \frac{S}{t+u+1} \left[ \frac{\ln t}{2} \left( 1 - \frac{1}{t^2} \right) + 1 - \frac{1}{t} - \frac{\ln t}{t+1} \right], \quad (7)$$

where  $u = U/B$ ,  $t = T/B$ ,  $S = 4\pi a_0^2 N R^2 / B^2$  ( $a_0 = 0.5292 \text{ \AA}$ ,  $R = 13.61 \text{ eV}$ ), and  $T$  is the energy of the impinging electron.

Finally, the total cross section for the electron-impact ionization  $\sigma^{\text{Ion}}$  can be obtained as

$$\sigma^{\text{Ion}} = \sum_{i=1}^{n_{\text{MO}}} \sigma_i^{\text{BEB}}, \quad (8)$$

where  $n_{\text{MO}}$  is the number of the given molecular orbital. The electron binding energy  $B$ , kinetic energy of the orbital  $U$ , and orbital occupation number  $N$  have been calculated for the ground states of the geometrically optimized, within  $C_{3v}$  symmetry, TMA molecule with the Hartree-Fock method using the GAUSSIAN code [27], and Gaussian 6-311G+(d,p) basis set. Because energies of the highest occupied molecular

TABLE II. Absolute electron-scattering total cross sections for  $\text{N}(\text{CH}_3)_3$  molecules in  $10^{-20} \text{ m}^2$ .

$E$ (eV)	TCS	$E$ (eV)	TCS	$E$ (eV)	TCS
0.8	23.7	6.3	56.2	27	45.0
1.0	23.7	6.5	56.2	30	43.7
1.2	23.9	6.8	57.2	35	41.6
1.4	24.1	7.1	58.1	40	40.6
1.6	24.4	7.3	58.7	45	39.6
1.8	24.8	7.5	59.4	50	38.3
2.0	25.2	7.8	59.8	60	35.7
2.2	25.8	8.1	59.7	70	33.9
2.4	26.5	8.3	59.8	80	32.6
2.6	27.4	8.5	60.4	90	30.7
2.8	28.5	8.8	61.3	100	29.6
3.1	30.6	9.3	60.9	110	28.4
3.3	32.6	9.8	60.3	120	27.1
3.5	33.9	10.3	59.5	140	24.1
3.8	37.0	10.8	58.8	160	22.2
4.1	39.7	11.3	58.4	180	20.5
4.3	41.7	12	57.4	200	18.6
4.5	43.2	13	55.8	220	17.3
4.8	45.8	14	53.9	250	15.7
5.1	47.5	16	50.6	270	14.7
5.3	49.8	18	49.0	300	13.5
5.5	51.4	20	47.6	350	12.2
5.8	53.5	23	46.6	370	11.9
6.1	55.3	25	45.7		

orbitals (HOMO) obtained this way can differ from the experimental ones, we also performed the outer valence Green's function calculations of correlated electron affinities and ionization potentials [28–31] using the GAUSSIAN code. The resulting computed values of the electron binding energies, kinetic energies of the orbitals, and orbital occupation number are listed and compared with other theoretical [32,33] and experimental [34–36] data, if available, in Table I. The agreement between the electron binding energies of the valence orbitals calculated in the present work and the experimental [34–36] is quite satisfactory.

The elastic (ECS) and ionization (ICS) calculated cross sections make it possible to estimate the computed total cross section for electron-TMA scattering as the sum of these partial cross sections. Although this approach seems to be rather crude, we expect that the total cross section (elastic + ionization) estimated this way will represent the electron-scattering TCS for TMA quite satisfactorily (to within  $\pm 10\%$ ). This expectation is justified by the results of our previous calculations which reproduced the experimental intermediate-energy data successfully for a variety of complex molecular targets [e.g.,  $\text{B}(\text{CD}_3)_3$  [37],  $\text{C}_4\text{H}_8\text{O}$  [38], and  $\text{C}_5\text{H}_{10}\text{O}_2$  [39], and references therein].

#### IV. RESULTS AND DISCUSSION

In this section we present our results for the total electron scattering cross section from trimethylamine  $\text{N}(\text{CH}_3)_3$ , mea-

TABLE III. Ionization (ICS), integral elastic (ECS), and summed (ECS+ICS) cross sections calculated for electron impact on  $\text{N}(\text{CH}_3)_3$  molecules; in  $10^{-20} \text{ m}^2$ .

$E$ (eV)	ICS	$E$ (eV)	ICS	ECS	ECS+ICS
8.397	0	30	7.75	42.1	49.9
9	0.971	35	8.93	36.6	45.5
10	0.267	40	9.79	32.5	42.3
11	0.435	45	10.4	29.4	39.8
12	0.595	50	10.8	26.9	37.7
13	0.760	60	11.3	23.2	34.5
14	1.08	70	11.5	20.5	32.0
15	1.53	80	11.5	18.5	30.0
16	2.0	90	11.4	17.0	28.4
17	2.52	100	11.2	15.7	26.9
18	3.06	110	11.0	14.6	25.6
19	3.58	120	10.7	13.8	24.5
20	4.07	140	10.2	12.3	22.6
22.5	5.18	160	9.76	11.2	21.0
25	6.15	180	9.30	10.3	19.6
27.5	7.00	200	8.86	9.54	18.4
		300	7.16	7.11	14.3
		400	6.00	5.74	11.7
		500	5.18	4.84	10.0
		600	4.57	4.19	8.76
		700	4.09	3.71	7.80
		800	3.71	3.33	7.04
		900	3.40	3.02	6.42
		1000	3.13	2.77	5.90
		2000	1.81	1.62	3.43
		3000	1.30	1.39	2.69

sured in the linear electron-transmission experiment over the energy range from 0.8 to 370 eV. These results are compared with our calculations and with TCS data for other nitrogen containing compounds,  $\text{NH}_3$  and  $\text{NH}_2\text{CH}_3$ .

#### A. Trimethylamine TMA, $\text{N}(\text{CH}_3)_3$

Figure 1 shows the variation of the absolute total electron-scattering cross sections for  $\text{N}(\text{CH}_3)_3$  over an energy range from 0.8 to 370 eV. The present data are obtained with the transmission method in which the reaction volume is free of electric and magnetic fields. The TCS measured from 1 to 49 eV by Schmieder in 1930 [4] with the Ramsauer “magnetic” technique is also displayed for comparison. Table II lists the numerical experimental TCS values taken in the present experiment. The computed cross sections of the integral elastic (ECS), total ionization (ICS), and their sum (ECS+ICS) are collected in Table III.

The most distinctive feature in the measured TCS is the strong enhancement peaked close to 9 eV. At low energies the cross section increases only slowly, from nearly  $24 \times 10^{-20} \text{ m}^2$  at 0.8 eV to about  $29 \times 10^{-20} \text{ m}^2$  near 3 eV. Thereafter, the cross section increases rapidly to reach its

maximum of  $61 \times 10^{-20} \text{ m}^2$  at 9 eV. Between 9 and 16 eV, the TCS falls rapidly and then more slowly down to a value of about  $12 \times 10^{-20} \text{ m}^2$  at 370 eV. The shape of the TCS curve around the maximum suggests that the pronounced enhancement might be composed of two structures: very broad hump centered between 15–25 eV and spanned over whole energy range applied, superimposed with the other much narrow peak around 9 eV. The large broad hump is most likely due to direct electron scattering. On the low-energy slope of the enhancement two weak supplementary features are discernible (see inset in Fig. 1): the first feature is barely visible near 6 eV, while the second one, more pronounced, is located around 8 eV. Although the magnitude of these features looks rather small, they were clearly perceivable in all experimental series. There are indications that the steeper part of the TCS enhancement (between 4 and 14 eV) must be, at least in part, related to the resonant scattering involving the formation of a temporary negative ion due to capture of the incident electron by target molecule into the unoccupied orbital. In the derivative electron-transmission spectra of gaseous TMA, Giordan *et al.* [9] and Tossell *et al.* [10] have revealed a broad resonance around 4.8 eV. Calculations [40] show that the lowest empty orbital of TMA molecule in the electronic ground state, to which the approaching electron could be attached, is located at 4.9 eV. The electron impact excitation spectra for five of the fundamental vibrations of TMA adsorbed on GaAs obtained by Mulcahy *et al.* [11] show the resonant behavior with an intense maximum centered within 5–6 eV, while the elastic spectrum peaks at 8 eV. Although the location of these structures and the weak features in the present TCS is the same, this coincidence may be quite fortuitous, as the dynamics of electron scattering from gaseous and adsorbed molecules is rather different. Further, indirect suggestion about the resonant contribution to the  $e\text{-N(CH}_3)_3$  TCS enhancement comes from comparison with other nitrogen-containing molecules in gas phase. Two low-energy resonances occur in  $\text{NH}_3$  (at 5.7 and 7.3 eV) [41] and two in  $\text{NH}_2\text{CH}_3$  (centered at 7.5 and 8.3 eV) [42]. Also TCS curves for these targets reveal in the resonant region an enhancement peaked within 7–9 eV (e.g., Refs. [43–45]), similar in general appearance to that for  $\text{N(CH}_3)_3$  (cf. Fig. 3). Lack of detailed  $e\text{-N(CH}_3)_3$  scattering data makes more extensive interpretation of the TCS behavior difficult.

Although the range of very low energies is out of the scope of the present experiment, it is worth mentioning here the result of Christophorou and Christodoulides [ $\sigma_m = 280 \times 10^{-20} \text{ m}^2$ , at thermal energies [6]] which points out that towards zero energy the cross section has to rise very sharply. That means somewhere below 1 eV the TCS has very deep Ramsauer-like minimum. Such high transparency of the TMA molecule in this energy range is related to the specific composition of electron-molecule interaction in which short-range, attractive polarization potential effects are important. However, the rapid increase of TCS at the close-to-zero energy [6] is in part connected also with the presence of the permanent dipole moment of TMA molecule (Table IV).

Figure 1 indicates that there is a general similarity, according to the shape, between the present experimental TCS

TABLE IV. Molecular electric dipole moments  $\mu$ , electric dipole polarizabilities  $\alpha$ , ionization potentials IP, and the gas-kinetic cross sections  $\sigma_{\text{gk}}$  for some nitrogen-containing molecules; data are from Ref. [47].

Molecule	$\mu$ (Debye)	$\alpha$ ( $10^{-30} \text{ m}^3$ )	IP (eV)	$\sigma_{\text{gk}}$ ( $10^{-20} \text{ m}^2$ )
$\text{N(CH}_3)_3$	0.612	8.15	7.82	15.5
$\text{NH}_2\text{CH}_3$	1.31	4.01	8.80	10.2
$\text{NH}_3$	1.47	2.10–2.81	10.07	7.94

energy function and the very old data of Schmieder [4]; both curves show very pronounced enhancement. It is immediately apparent, however, that the position of the maximum in the curve of Schmieder is distinctly shifted towards lower energy by about 1–1.5 eV. A similar shift has been observed when comparing data for other targets collected in the present apparatus with that reported by Schmieder (cf. Refs. [44,46]). One possible reason for this disagreement is a systematic error in determining the energy scale in the older experiment. One can also see from Fig. 1 that the curve of Schmieder does not reveal any structure on the left-hand side of the TCS enhancement, likely due to the poorer energy resolution. As to the magnitude, there is a distinct disagreement between two compared experimental TCS energy dependences. While between 2 and 20 eV the difference does not exceed 12%, close to 1 and 50 eV the disaccord reaches 25%. A possible cause of this disagreement is that the early measurements with the Ramsauer technique may have significantly suffered from systematic forward-scattering effect, resulting in a smaller value of the measured TCS (in Refs. [44,46]).

Figure 2 shows the integral elastic  $e\text{-TMA}$  cross section (ECS) computed in the independent atom approximation and

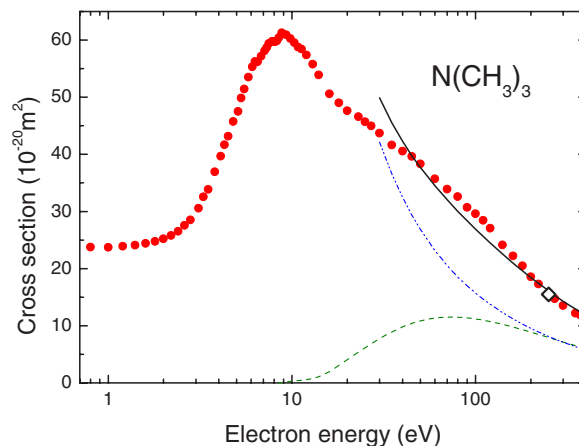


FIG. 2. (Color online) Comparison of the measured total  $e\text{-N(CH}_3)_3$  cross section (full circles) with cross sections calculated in the present work: integrated elastic (dash double-dotted line) in the IAM approach with the SP potential; total ionization (dashed line) in the BEB approximation; the sum of elastic and ionization cross sections (full line). Open diamond (at 250 eV) represents the gas-kinetic cross section estimated from the van der Waals constant  $b$  [47].

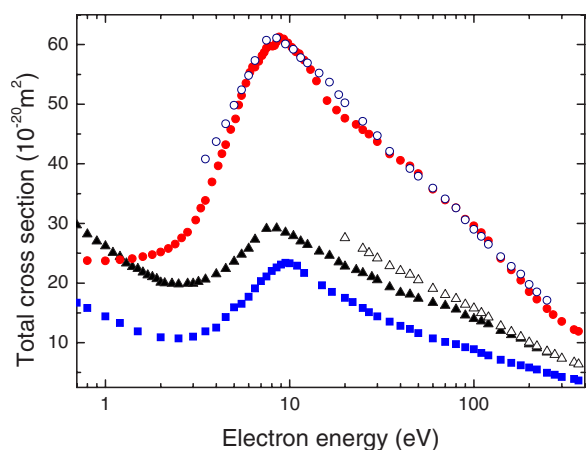


FIG. 3. (Color online) Comparison of the experimental electron-scattering TCS for some nitrides:  $\text{N}(\text{CH}_3)_3$  (full circles), present;  $\text{NH}_2\text{CH}_3$  (full triangles), from Ref. [44];  $\text{NH}_3$  (full squares), from Refs. [43,45]. There are shown also examples of some TCS estimations (see text): for  $\text{N}(\text{CH}_3)_3$  (open circles) as the sum of TCSs for  $\text{NH}_2\text{CH}_3$  and  $\text{C}_2\text{H}_4$  [49], while TCS for  $\text{NH}_2\text{CH}_3$  (open triangles) is composed as  $1/3 \times \text{TCS}_{\text{N}(\text{CH}_3)_3} + 2/3 \times \text{TCS}_{\text{NH}_3}$ .

the total ionization cross section (ICS) calculated in the binary-encounter-Bethe approach. It is interesting that above 200 eV both partial cross sections contribute equally to the  $e$ -TMA scattering; their sum (ECS+ICS) is also shown in Fig. 2 and compared with the TCS measured in the present work. The agreement of the summed cross section with the experimental TCS is satisfactory; above 40 eV, where with increasing energy the assumptions of IAM approximation become to be fulfilled better and better, the computed and measured TCSs do not differ more than 8%.

Based on the van der Waals constant  $b$  [47] we have also estimated the gas-kinetic cross section for TMA,  $\sigma_{\text{gk}} = 15.5 \times 10^{-20} \text{ m}^2$ , this value fairly well represents the electron-scattering TCS around 250 eV. Similar agreement of the gas kinetic and the experimental total electron-scattering cross sections has been already noticed between 200 and 300 eV for a number of hydrogen-containing molecules (e.g., [48]).

#### B. Comparison of TCSs for nitrogen-containing compounds: $\text{NH}_3$ , $\text{NH}_2\text{CH}_3$ , and $\text{N}(\text{CH}_3)_3$

Figure 3 compares the TCS for electron scattering from three nitrogen-containing molecules: for  $\text{NH}_3$  (from Refs. [43,45]), for its permethylated analog  $\text{N}(\text{CH}_3)_3$  (present), and for  $\text{NH}_2\text{CH}_3$  [44]. Regarding the shape, around 9 eV the compared TCS curves resemble each other; they all have distinct enhancement with the maximum located within 7–9 eV.

The only evident difference in the TCS behavior is visible below 2 eV where TCS curves for more polar targets (cf. Table IV),  $\text{NH}_3$  and  $\text{NH}_2\text{CH}_3$ , increases when the energy decreases. The variation in the TCS magnitude, when going from one target to another, can be explained in terms of the different molecular size of target molecules.

Finally, an analysis of the existing experimental electron-scattering TCS data for these nitrides was made with an at-

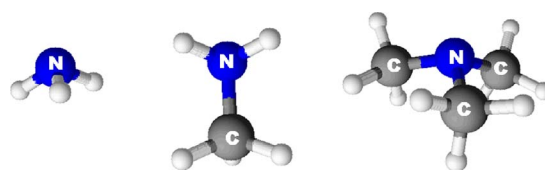


FIG. 4. (Color online) Schematic of  $\text{NH}_3$ ,  $\text{NH}_2\text{CH}_3$ , and  $\text{N}(\text{CH}_3)_3$  geometry.

tempt to find any relationship between them. The problem is of practical interest, because if such relationship exists, it may greatly help in the easy estimation of cross sections for some of those molecular targets for which the experiments and computations are still difficult to perform. A promising method is to compose the TCS for a molecule as the sum of cross sections for groups of atoms which constitute the complex molecule under study. Figure 3 shows that beyond 5 eV the TCS for  $\text{N}(\text{CH}_3)_3$  is reasonably estimated just as the sum of TCSs for  $\text{NH}_2\text{CH}_3$  and  $\text{C}_2\text{H}_4$  (data taken from Ref. [44,49], respectively); note that the  $\text{N}(\text{CH}_3)_3$  molecule has the same constituent atoms as  $\text{NH}_2\text{CH}_3$  together with  $\text{C}_2\text{H}_4$ . Surprising is the fact that in this particular case the summed cross section reproduces the TCS over such a wide energy range; typically, it is roughly satisfied well above 100 eV [37,45,48]. Another interesting observation, which results from simple geometrical considerations (see Fig. 4), is that the gas-kinetic cross section (see in Table IV), and to some extent also the total (above 50 eV) cross section for any of three nitrides [ $\text{NH}_3$ ,  $\text{NH}_2\text{CH}_3$ , and  $\text{N}(\text{CH}_3)_3$ ] can be estimated as a combination of cross sections for fragments of these molecules: e.g., the TCS for  $\text{NH}_2\text{CH}_3$  equals  $1/3$  of the TCS for  $\text{N}(\text{CH}_3)_3$  plus  $2/3$  of the TCS for  $\text{NH}_3$ . It means that having data for appropriate molecular segments only, one may roughly estimate the cross section for a given molecule as a whole before measurements and/or calculations are carried out. In the aforementioned case, the TCS for  $\text{NH}_2\text{CH}_3$  above 250 eV, with lack of other data, can also be predicted reasonably (see Fig. 3). Additionally, one may suppose that such regularity may also shed light onto the specific role of atomic groups in scattering process.

#### V. SUMMARY

We have presented the absolute total electron-scattering cross section for the  $\text{N}(\text{CH}_3)_3$  molecule measured in a linear transmission experiment from 0.8 to 370 eV. The experimental TCS energy dependence for  $\text{N}(\text{CH}_3)_3$  shows a very distinct enhancement peaked near 9 eV, overlapped with two weak features at 6.5 and 8 eV. The data are in qualitative agreement with the only previous results recorded by Schmieder [4] in the energy range of overlap. We have also carried out calculations of the integral elastic, total ionization, and total (elastic+ionization) cross sections from intermediate up to 3 keV impact energies. Good agreement between the present computed and experimental intermediate-

energy total cross sections suggests that the approximate IAM and BEB methods adopted here look promising for the prediction of the reasonable cross sections for such complex targets. Additional experimental and theoretical studies are required for particular electron scattering processes (e.g., elastic and vibrational differential cross sections).

#### ACKNOWLEDGMENTS

This work is part of the MNiSzW Project 2007–2008 and is supported by the Polish Ministry of Science and Higher Education (Project No. N202 110 32/2862). Numerical calculations have been performed at the Academic Computer Center (TASK) in Gdańsk.

- 
- [1] K. Mitsubayashi and Y. Hashimoto, *IEEE Sens. J.* **2**, 133 (2002).
- [2] W. Tanthapanichakoon, P. Khongprasamkain, T. Charinpanitkul, H. Tamon, N. Sano, and M. Okazaki, *ScienceAsia* **25**, 57 (1999).
- [3] I. Guest and D. R. Varma, *J. Toxicol. Environ. Health* **36**, 27 (1992).
- [4] F. Schmieder, *Z. Elektrochem. Angew. Phys. Chem.* **36**, 700 (1930).
- [5] B. Beagley and T. G. Hewitt, *Trans. Faraday Soc.* **64**, 2561 (1968).
- [6] L. G. Christophorou and A. A. Christodoulides, *J. Phys. B* **2**, 71 (1969).
- [7] B. H. Solka and M. E. Russell, *J. Phys. Chem.* **78**, 1268 (1974).
- [8] A. G. Loudon and K. S. Webb, *Org. Mass Spectrom.* **12**, 283 (1977).
- [9] J. C. Giordan, J. H. Moore, J. A. Tossell, and W. Kaim, *J. Am. Chem. Soc.* **107**, 5600 (1985).
- [10] J. A. Tossell, J. H. Moore, and J. C. Giordan, *Inorg. Chem.* **24**, 1100 (1985).
- [11] C. P. A. Mulcahy, A. A. Aquino, J. J. Rogers, and T. S. Jones, *J. Chem. Phys.* **104**, 9120 (1996).
- [12] B. M. Davies and J. H. Craig, Jr., *Surf. Interface Anal.* **35**, 1060 (2003).
- [13] J. Lozano, D. Early, J. H. Craig, Jr., P. W. Wang, and K. R. Kimberlin, *Surf. Interface Anal.* **37**, 366 (2005).
- [14] Cz. Szmytkowski, P. Możejko, and G. Kasperski, *J. Phys. B* **31**, 3917 (1998).
- [15] Cz. Szmytkowski and P. Możejko, *Vacuum* **63**, 549 (2001).
- [16] M. Knudsen, *Ann. Phys.* **31**, 205 (1910).
- [17] R. N. Nelson and S. O. Colgate, *Phys. Rev. A* **8**, 3045 (1973).
- [18] N. F. Mott and H. S. W. Massey, *The Theory of Atomic Collisions* (Oxford University Press, Oxford, 1965).
- [19] Y.-K. Kim and M. E. Rudd, *Phys. Rev. A* **50**, 3954 (1994).
- [20] W. Hwang, Y.-K. Kim, and M. E. Rudd, *J. Chem. Phys.* **104**, 2956 (1996).
- [21] P. Możejko, B. Żywicka-Możejko, and Cz. Szmytkowski, *Nucl. Instrum. Methods Phys. Res. B* **196**, 245 (2002).
- [22] P. Możejko and L. Sanche, *Radiat. Environ. Biophys.* **42**, 201 (2003).
- [23] F. Salvat, J. D. Martinez, R. Mayol, and J. Parellada, *Phys. Rev. A* **36**, 467 (1987).
- [24] N. T. Padial and D. W. Norcross, *Phys. Rev. A* **29**, 1742 (1984).
- [25] J. P. Perdew and A. Zunger, *Phys. Rev. B* **23**, 5048 (1981).
- [26] X. Zhang, J. Sun, and Y. Liu, *J. Phys. B* **25**, 1893 (1992).
- [27] M. J. Frisch *et al.*, *GAUSSIAN 03*, Revision B.05 (Pittsburgh: Gaussian, 2003).
- [28] L. S. Cederbaum, *J. Phys. B* **8**, 290 (1975).
- [29] W. von Niessen, J. Schirmer and L. S. Cederbaum, *Comput. Phys. Rep.* **1**, 57 (1984).
- [30] J. V. Ortiz, *J. Chem. Phys.* **89**, 6348 (1988).
- [31] V. G. Zakrzewski and W. von Niessen, *J. Comput. Chem.* **14**, 13 (1994).
- [32] L. Noodleman and N. L. Paddock, *Inorg. Chem.* **18**, 354 (1979).
- [33] K. McMillan, M. A. Coplan, J. H. Moore, and J. A. Tossell, *J. Phys. Chem.* **94**, 8648 (1990).
- [34] K. Kimura and K. Osafune, *Mol. Phys.* **29**, 1073 (1975).
- [35] A. W. Potts, T. A. Williams, and W. C. Price, *Discuss. Faraday Soc.* **54**, 104 (1972).
- [36] A. B. Cornford, D. C. Frost, F. G. Herring, and C. A. McDowell, *Can. J. Chem.* **49**, 1135 (1971).
- [37] A. Domaracka, P. Możejko, E. Ptasińska-Denga, and Cz. Szmytkowski, *J. Phys. B* **39**, 4289 (2006).
- [38] P. Możejko, E. Ptasińska-Denga, A. Domaracka, and Cz. Szmytkowski, *Phys. Rev. A* **74**, 012708 (2006).
- [39] P. Możejko, A. Domaracka, E. Ptasińska-Denga, and Cz. Szmytkowski, *Chem. Phys. Lett.* **429**, 378 (2006).
- [40] E. Lindholm, L. Asbrink, and S. Ljunggren, *J. Phys. Chem.* **95**, 3923 (1991).
- [41] M. Tronc, R. Azria, and M. Ben Arfa, *J. Phys. B* **21**, 2497 (1988).
- [42] F. Motte-Tollet, M.-J. Hubin-Franskin, and J. E. Collin, *J. Chem. Phys.* **93**, 7843 (1990).
- [43] Cz. Szmytkowski, K. Maciag, G. Karwasz, and D. Filipović, *J. Phys. B* **22**, 525 (1989).
- [44] Cz. Szmytkowski and A. M. Krzysztofowicz, *J. Phys. B* **28**, 4291 (1995).
- [45] Cz. Szmytkowski, M. Piotrowicz, A. Domaracka, Ł. Kłosowski, E. Ptasińska-Denga, and G. Kasperski, *J. Chem. Phys.* **121**, 1790 (2004).
- [46] Cz. Szmytkowski and S. Kwitniewski, *J. Phys. B* **35**, 3781 (2002).
- [47] *CRC Handbook of Chemistry and Physics*, 86th edition, edited by D. R. Lide (Taylor and Francis, Boca Raton, 2006), CD-ROM Version 2006.
- [48] Cz. Szmytkowski, Ł. Kłosowski, A. Domaracka, M. Piotrowicz, and E. Ptasińska-Denga, *J. Phys. B* **37**, 1833 (2004).
- [49] Cz. Szmytkowski, S. Kwitniewski, and E. Ptasińska-Denga, *Phys. Rev. A* **68**, 032715 (2003).